Cement and Concrete Research 42 (2012) 539–548

Contents lists available at SciVerse ScienceDirect

Cement and Concrete Research

journal homepage: http://ees.elsevier.com/CEMCON/default.asp

TiO_2 photocatalysis in cementitious systems: Insights into self-cleaning and depollution chemistry

Andrea Folli [a,*], Claus Pade [b], Tommy Bæk Hansen [c], Tiziana De Marco [d], Donald E. Macphee [a,*]

[a] University of Aberdeen, Meston Building, Meston Walk, AB24 3UE, Aberdeen, Scotland, UK
[b] DTI, Byggeri - Beton, Gregersensvej, Høje Tåstrup, Denmark
[c] Aalborg Portland A/S, Product Technology, Sølystvej 18, 9220 Aalborg Ø, Denmark
[d] CTG-Italcementi Group, Via Camozzi 124, Bergamo, 24121, Italy

ARTICLE INFO

Article history:
Received 27 May 2010
Accepted 2 December 2011

Keywords:
TiO_2 photocatalysis
Self-cleaning
Aesthetic durability
Depollution
Particle size

ABSTRACT

The present work offers a general overview about application of titanium dioxide (or titania), TiO_2, photocatalysis to concrete technology in relation to enhanced aesthetic durability and depollution properties achieved by implementing TiO_2 into cement. Chemistry of degradation of Rhodamine B (RhB), a red dye used to assess self-cleaning performances of concretes containing TiO_2, as well as oxidation of nitrogen oxides (NOx), gaseous atmospheric pollutants responsible for acid rains and photochemical smog, is investigated using two commercial titania samples in cement and mortar specimens: a microsized, m-TiO_2 (average particle size 153.7 nm ± 48.1 nm) and a nanosized, n-TiO_2 (average particle size 18.4 nm ± 5.0 nm). Experimental data on photocatalytic performances measured for the two samples are discussed in relation to photocatalyst properties and influence of the chemical environment of cement on titania particles. Impacts on applications in construction concrete are also discussed.

1. Introduction

The photochemistry of TiO_2 has become a subject of intense research since Fujishima and Honda [1] and Wrighton et al. [2] reported the photocatalytic splitting of water on TiO_2 and Sr-doped TiO_2 respectively in the 1970s. Applications of TiO_2 photocatalysts to construction materials began towards the end of the 1980s. Two important effects related to the nature of photoactive TiO_2 coatings had by this time been discovered: a) the self-cleaning effect due to redox reactions promoted by sunlight (or in general, weak U.V. light) on the photocatalyst surface [3], and b) the photo-induced hydrophilicity [4,5] of the catalyst surface, which enhances the self-cleaning effect (inorganics causing dirt and stains on surfaces can be easily removed due to rainwater soaking between the adsorbed substance and the TiO_2 surface). Photocatalytic glasses provide an example of self-cleaning and anti-fogging (wetting) properties, e.g. Pilkington Active™ [6]. Recently, photocatalytic cementitious materials have been patented by Mitsubishi Corp.(NOxer™), and Italcementi SpA (TX-Aria™ and TX-Arca™) [7–10]. The application of TiO_2 photocatalysis to concrete aims to achieve two main goals, the self-cleaning effect discussed above and the *depolluting* effect due to the oxidation of nitrogen oxides (NO_x) in the atmosphere to NO_3^-, especially in street canyons where NO_x concentrations can be considerable due to combustion engine exhausts. The great advantage provided by such products is that the only requirements, beyond TiO_2 in the construction material used, are sunlight, oxygen and water.

1.1. Self-cleaning and aesthetic durability

Development of TiO_2–cementitious binders providing self-cleaning has been carried out in order to enhance aesthetic durability of cementitious materials, particularly those based upon white cement. Although the use of such products is still restricted and limited, many buildings have been designed and constructed since 2000, to fulfil high aesthetic standards. Relevant examples are: Church "Dives in Misericordia", Rome, ITALY, Music and Arts City Hall, Chambéry, FRANCE, Police Central Station , Bordeaux, FRANCE, Air France Building, Roissy-Charles de Gaulle Airport, FRANCE, Saint John's Court, Montacarlo, MONACO.

In order to verify self-cleaning performances of photocatalytic cements/concretes, several tests involving organic substances have been set up and include the degradation of colour in dyes. Rhodamine B (*N-[9-(2-Carboxyphenyl)-6-diethylamino-3H-xanthen-3-ylidene]-N-ethyl-ethanaminium chloride*) is one of the most common dye tests and is adopted as an Italian standard (UNI 11259 (February 2008) [11]). Rhodamine B, RhB, degradation on TiO_2 surfaces has been extensively studied in slurry systems (TiO_2 suspended in aqueous solutions of RhB) under different illumination conditions [12–16]. Results have shown efficient degradation of colour under both U.V. light and visible light. Under U.V. light illumination RhB is degraded by an ordinary *TiO_2-sensitised photoreaction* [12,17]: a TiO_2 photocatalytic

* Corresponding authors.
E-mail addresses: a.folli@abdn.ac.uk (A. Folli), d.e.macphee@abdn.ac.uk (D.E. Macphee).

0008-8846/$ – see front matter © 2011 Elsevier Ltd. All rights reserved.
doi:10.1016/j.cemconres.2011.12.001

process involving photon absorption and electron promotion from the valence band, leaving positive holes, to the conductance band of the semiconductor (Fig. 1). Under visible light illumination, RhB undergoes a *dye-sensitised* photoreaction [12,17]: the organic molecule absorbs visible light photons which can only promote electrons from the highest occupied molecular orbital (HOMO) to the lowest unoccupied molecular orbital (LUMO) in the organic molecule since they do not possess enough energy to activate TiO_2 (band gap in the near UV). These electrons are further injected from the RhB LUMO to the conductance band of TiO_2, leading to the formation of RhB^+ molecular ion radicals on the TiO_2 surface. The transfer of the conductance band electron to adsorbed oxygen on the TiO_2 surface produces O_2^-. Both radical species arising from this process are highly reactive leading ultimately to mineralization of the organic molecule (Fig. 2) [12,13].

1.2. Depollution

Air pollution due to *nitrogen oxides* (NOx) is a dramatic issue that modern societies are facing. They are amongst the main responsible for *photochemical smog* [18] (mixture of hazardous chemicals formed in the atmosphere due to interaction of sunlight with already present pollutants); together with sulphur oxides (SOx) they generate acid rains [18–20]; direct exposures or acid vapours generated by reaction with atmospheric moisture can cause emphysemas and bronchitis due to their interaction with lung tissues [18] and, not least, they seriously affect plant regular metabolism [18]. In atmospheric chemistry NOx refers to the sum of nitric oxide, NO, and nitrogen dioxide, NO_2. NO is considered a *primary* pollutant [18] because mainly introduced in the atmosphere directly from a source (high temperature combustions in transport and industrial activities [18–21]). NO_2, on the other hand, is considered as a *secondary* pollutant because mainly formed in the atmosphere by interaction of a primary pollutant (NO) with O_2 (or O_3) and/or sunlight [18–21]. Further reactions in the atmosphere can transform NO and NO_2 in nitric acid, HNO_3, peroxyacyl nitrates (PANs), $RC(O)OONO_2$, peroxynitric acid, HNO_4, etc… The sum of all these species and NOx is known as NOy, *total reactive nitrogen*.

NOx emission has been and still is subject of intense environmental regulations. Therefore their control and remediation have been the subject of intense research. Amongst the most used technologies for NOx remediation (combustions modifications, dry processes and wet processes [22,23]) photocatalytic oxidation (PCO) of NOx has become, over the past ten years, a valid alternative as confirmed by the large number of literature produced [17,24–36] and the continuous growing number of commercial products available in the market. These products are essentially paints or cements containing photoactive TiO_2 [7,37,38], photocatalytic pavement blocks [8], filters and membranes for indoor/outdoor air purifications, etc… Despite all the other technologies, PCO provides the great advantage to promote NOx oxidation on the surface of light activated TiO_2 using only atmospheric oxygen and water.

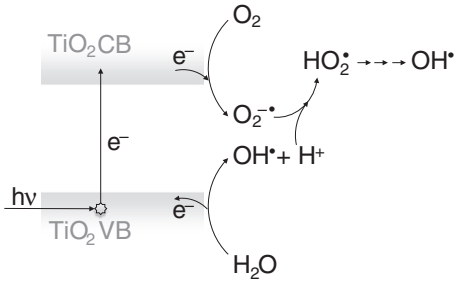

Fig. 1. RhB–TiO_2 system under U.V. light irradiation: *TiO_2-sensitised* pathway [12].

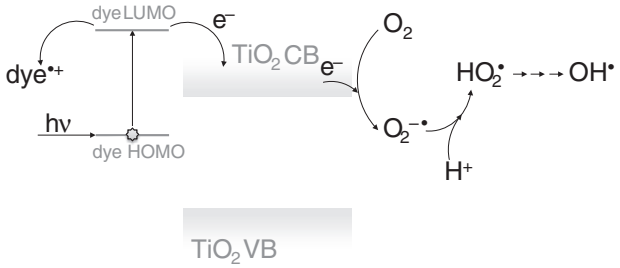

Fig. 2. RhB–TiO_2 system under visible light irradiation: *dye-sensitised* pathway [12].

Depolluting performances of cementitious materials containing TiO_2 are usually assessed in gas flow reactors with a photocatalytic bed consisting in the concrete specimen to be analysed. Reactors are fed with air streams containing nitrogen oxides at a given partial pressure and NO and NO_2 concentrations are monitored in darkness and under illumination [24,25,34,39]. Alternatively, *real world exposure* tests offer a mean to address performances in actual outdoor conditions, by monitoring the concentration drop of NOx in the air where photocatalytic concrete is used as pavement blocks or in vertical walls [9,24,29].

2. Experimental

2.1. TiO_2 samples

Throughout this study, two commercially available titanias: *m-TiO_2* (microsized, Huntsman Tioxide Pigments A-HR) and *n-TiO_2* (nanosized, Millenium Chemicals PC-105), both 100% anatase, have been tested. Before starting any degradation experiments, these samples have been characterised in order to evaluate their main physical–chemical properties such as: light absorption characteristics, mineralogy, specific surface area, porosity and particle size. Light absorption measurements were undertaken to derive band-gap information and have been carried out on TiO_2 powders using U.V.–vis diffuse reflectance spectroscopy (StellarNet EPP2000 Spectrometer). Spectra were processed according to the Kubelka-Munk transform approach for indirect semiconductors as described in [40]. X-Ray Diffraction patterns have been obtained using a Bruker D8 Advance diffractometer equipped with a $Cu_{K\alpha 1}$ 1.54 Å X-Ray source operating at room temperature, in order to confirm the mineralogy and crystallinity. BET (Brunauer-Emmett-Teller [41]) specific surface area (S_{BET}) has been obtained by N_2 adsorption on powder samples using a Micromeritics ASAP 2020. These data enabled characterisation of sample porosity as determined by the BJH (Barrett-Joyner-Halenda) model [42], assuming cylindrical pores. Samples were degassed at 150 °C before adsorption measurements. Finally, particle size evaluation was carried out by three different techniques: TEM imaging (and further image analysis), XRD via the Scherrer Equation (Eq. (1)) and a simple geometrical model derived from the BET specific surface area assuming particles to be rigid spheres (Eq. (2)).

$$d = \frac{0.9 \cdot \lambda}{FWHM \cdot \cos\theta_P} \tag{1}$$

$$d = \frac{6}{\rho_A \cdot S_{BET}} \tag{2}$$

In Eq. (1): λ is the X-ray wavelength, FWHM, the full width at half maximum height for the anatase 101 peak at 25.2° (2θ), θ_P, the Bragg's diffraction angle for the same peak. In Eq. (2): ρ_A is the density of anatase taken as 3.895 g cm^{-3}, and S_{BET}, the BET specific surface area.

2.2. Aesthetic durability: self-cleaning performances (RhB test)

Two sets of photocatalytic cement pastes were prepared, one for each of the two commercial TiO_2 products. The TiO_2 and fresh white Portland cement (CEM I 52.5 R) powders were dry mixed in the mass ratio 3.5 : 96.5. 20 g of the mixture was subsequently hydrated with 8 g of distilled water (water:cement ratio, w/c = 0.4). A third set (control) was prepared without photocatalyst. After mixing, pastes were cast in 42 mm diameter moulds and cured for one day at room temperature and 80.5% relative humidity (over a saturated solution of $(NH_4)_2SO_4$). Six cement discs were produced for each set.

After one day of curing, all samples were coated with 20 μl of aqueous RhB solution (1.0 g l^{-1}). The coating area was approximately 1.2 cm^2. Three of the six discs per set were conditioned for 30 min under daylight, the remaining three were coated and conditioned for 30 min in darkness. All three sets were subsequently irradiated with a UVItec LI-208.m lamp (2 tubes 8 W each, main wavelength 312 nm) and reflectance measurements were performed after various illumination times using a StellarNet EPP2000 Spectrometer.

2.3. Depollution: NOx oxidation

Mortar samples for the NOx oxidation test have been prepared according to the procedure described in the European Standard ISO 679 [43]. In this case mortars were cast in 9 cm diameter × 1 cm thickness plastic Petri dishes. Three sets of twelve mortar discs each were produced: one with m-TiO_2, one with n-TiO_2 and one without photocatalyst as a control. Samples were cured for seven days at room temperature in sealed plastic bags and further seven days at room temperature and 60% of relative humidity.

NOx oxidation experiments have been carried out in a continuous gas flow reactor according to the Italian Standard UNI 11247 [34]. The scheme of the lab plant used is illustrated in Fig. 3. S1 is the NOx cylinder, S2 the air cylinder, F and FC the mass flow meters for NOx and air respectively, R the photocatalytic reactor, A the chemiluminescence analyzer and E the software/computer system for the analyzer. The photocatalytic reactor consists of a Pyrex glass chamber having a total volume of 3.58 l where the specimen under testing can be located on the bottom part supported by a proper sample holder. The gas inlet tube allows the air/NOx mixture to flow directly onto the specimen upper surface whilst the gas outlet tube is positioned underneath the sample holder. The system is kept at room temperature. U.V. light is provided by an OSRAM ULTRAVITALUX lamp having a main emission in the U.V.–A field distributed around a maximum intensity wavelength of about 365 nm. The lamp–sample distance was set to achieve on the upper sample surface an average irradiance of 20 ± 1 W m^{-2}. A schematic diagram of the photocatalytic reactor equipped with the U.V. lamp is illustrated in Fig. 4. Experiments were carried out at an inlet NO concentrations of 600 ppb in air with a ratio NO/NO_2 equal to 2 at three different flow rates: 3 l min^{-1}, 2 l min^{-1} and 1.5 l min^{-1}. All the oxidation experiments have been performed according to the following procedure. The disk

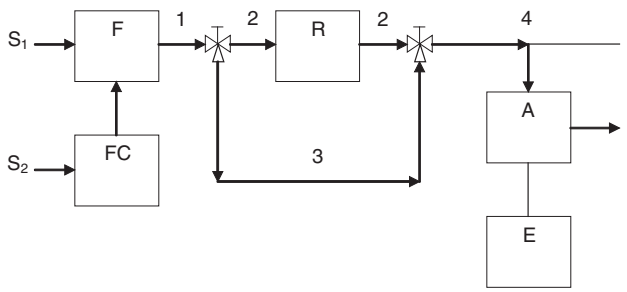

Fig. 3. NOx oxidation lab plant flow chart. S1 NOx cylinder, S2 air cylinder, F NOx flow meter, FC air flow meter, R photocatalytic reactor, A NOx analyser, E computer.

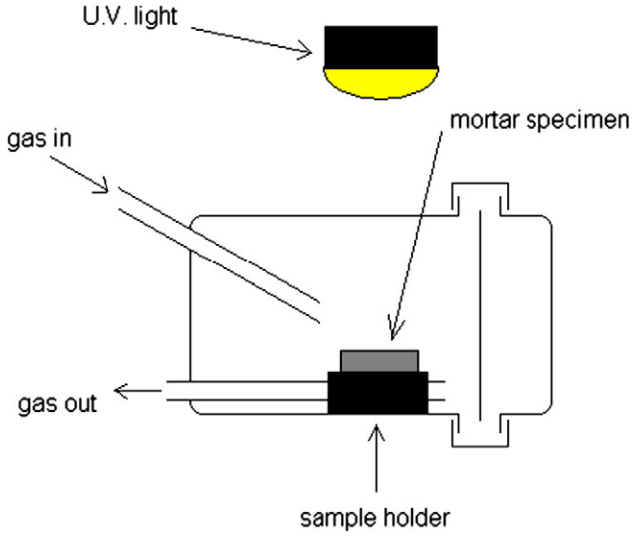

Fig. 4. Photocatalytic reactor for NOx oxidation.

sample was wrapped in a sealing film in order to let the upper surface free and protect the side surface. After introducing the disk sample in the photocatalytic reactor the gas stream (at given flow rate) was switched on and the system let to stabilise for half an hour in the dark in order to achieve constant NO and NO_2 concentrations. The U.V. light was then switched on and the NO, NO_2 concentrations monitored for a further 90 min.

3. Results and discussion

3.1. TiO_2 samples

Light absorption characteristics for both the photocatalysts are shown in Fig. 5 (a) and (b) presenting the Kubelka-Munk transformed function derived from the UV–vis Diffuse Reflectance Spectra for the untreated TiO_2 powders, a common approach to derive band

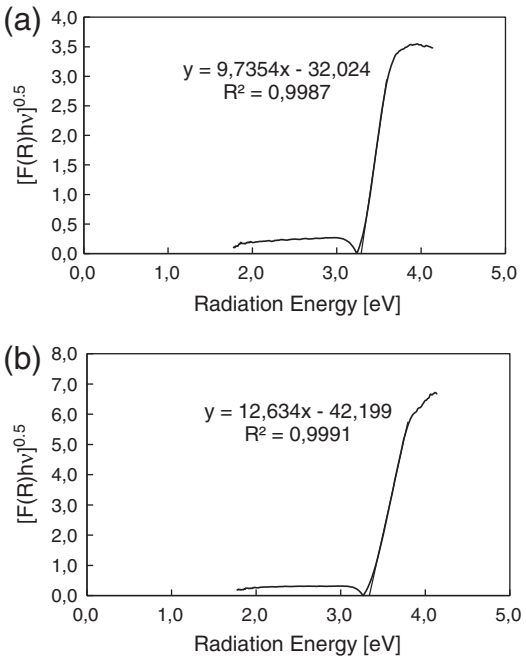

Fig. 5. Light absorption edges for m-TiO_2 (a) and n-TiO_2 (b) expressed through the Kubelka-Munk transform approach for indirect semiconductors; the band gap is derived by extrapolating the linear portion of the spectrum on the x-axis.

Table 1
TiO_2 physical characterisation data.

Sample	Crystalline Phase	Band Gap	S_{BET}	BJH Φ_{pore}	Particle size			
					Product spec	TEM	XRD	BET
		eV	m^2g^{-1}	*Å*	*nm*	*nm*	*nm*	*nm*
m-TiO_2	100% Anatase	3.29 ± 0.02	8.7	> 500	170	153.7 ± 48.1	–	177.6
n-TiO_2	100% Anatase	3.34 ± 0.02	78.9	79.6	17	18.4 ± 5.0	16.6 ± 2.0	19.5

gap of indirect semiconductors [40]. The computed band gap values are reported in Table 1. The values are typical of anatase samples [40]. The results of X-ray diffraction analyses are shown in Fig. 6. The peak positions confirm that both commercial TiO_2 products are essentially anatase [44,45]. Surface area data are presented in Fig. 7(a). The much lower level of N_2 adsorption on the microsized sample is consistent with this sample showing larger crystallites than the nanosized product as expected, and indeed, the BJH analysis (Fig. 7(b)) shows that considerable agglomeration has occurred in the nanosized sample under the conditions of testing, i.e. the pores arise from inter-particle volume. The corresponding porosity data cannot be obtained for the microsized sample as pore sizes are outside the measurable range.

Fig. 8 shows transmission electron micrograph images of both products. Again the crystallite size difference between the two samples is evident and this is quantitatively supported by the histograms shown as insets in the figure. The above data are summarised in Table 1. There is good agreement between the techniques and the results are consistent with manufacturers' data on particle size.

3.2. Aesthetic durability: self-cleaning performances (RhB test)

The degradation of colour of RhB (structure in Fig. 9) was semi-quantitatively measured by light absorption as a function of wavelength by reflecting light from the cement surface on which the dye is deposited (U.V.–vis Diffuse Reflectance Spectroscopy). Figs. 10, 11 and 12 show the spectra obtained. The peak area of the main absorption centred on 541.5 nm is indicative of the concentration of the dye molecule and it can be observed that under illumination, the area reduces as a function of time, i.e. the dye molecule degrades. It can be noted that there is also degradation of colour in samples which do not contain photocatalyst and this highlights an important source of misrepresentation of catalyst efficiency where controls are not used. The loss of colour by photolytic degradation of the dye is quite common, in fact this effect is observed as coloured fabrics are bleached in sunlight. However, even by taking account of this effect, it can be shown that there is an enhanced degradation of colour in the presence of photocatalyst [46]. This proves the self-cleaning effect of cement surfaces if TiO_2 is present in the structure.

An interesting feature of these data is the shift to lower wavelengths of absorption maxima exhibited by samples which experienced exposure to daylight during the dye deposition step. This feature is not reproduced when dye is deposited in the dark. A similar effect (hypsochromic shift or blue shift, i.e. shift of the absorption band towards lower wavelengths) was observed by Chen et al. in slurry systems [13], who discriminated between different degradation mechanisms as a function of the different illumination conditions experienced. The lower energies available from visible light are insufficient to induce photo-activation of TiO_2 but they can lead to dye sensitisation and degradation of colour by this mechanism. As a result, the selective stepwise de-ethylation of RhB amino groups responsible for the hypsochromic shift, leads to a sequence of structurally similar degradation products which absorb radiation at progressively lower wavelengths [13]. Where samples were prepared in the dark, the only light exposure was to UV radiation which promotes true photocatalytic processes [3,17] which, in the case of RhB mineralization, have been observed to be not selective (reduction of the hypsochromic shift) [13,46]. Clearly, degradation mechanisms are important in understanding optimisation of photocatalyst efficiencies. However, it is evident from the above that photocatalysis can encompass more than one process. Whilst UV exposure promotes conventional photocatalysis-induced redox processes on the surface of TiO_2, diagnosis of reaction pathways is complicated by the dye sensitisation mechanism and the influence of resulting products. A further physical implication is the particle size of the photocatalysts. m-TiO_2 performed better than n-TiO_2 (RhB deposited under day light conditions) or at least same as n-TiO_2 (RhB deposited in darkness), see Figs. 11 and 12. According to the BET specific surface areas, 8.7 $m^2\,g^{-1}$ for m-TiO_2 and 78.9 $m^2\,g^{-1}$ for n-TiO_2, and particle sizes, about 150 nm for m-TiO_2 and about 18 nm for n-TiO_2, the latter is expected to exhibit much higher activities due to higher surface area for adsorption of the RhB and much lower electron–hole recombination in the particles volume. However, considering that: i) the degradation of RhB, as described above, is a combination of conventional TiO_2-sensitised and dye-sensitised which (the latter) does

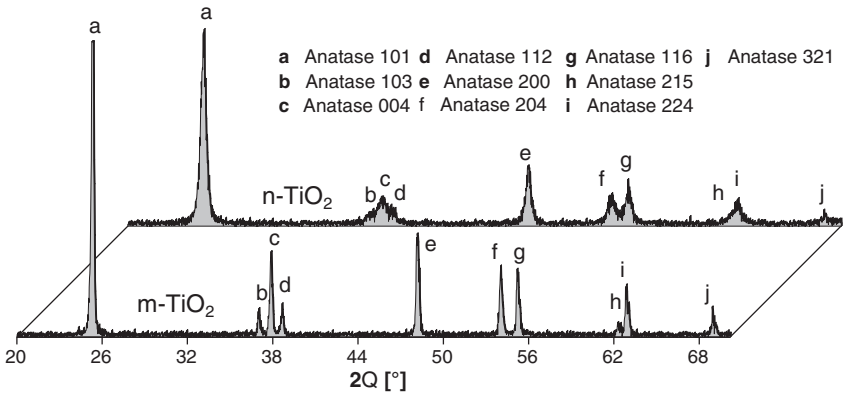

Fig. 6. Comparison of XRD patterns for m-TiO_2 and n-TiO_2.

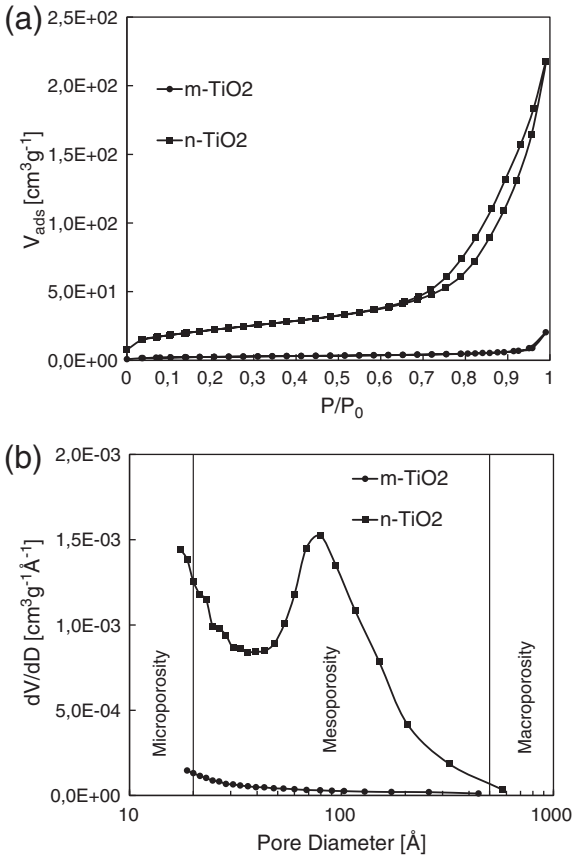

Fig. 7. (a) N_2 adsorption isotherms; and (b) BJH plot for porosity evaluation.

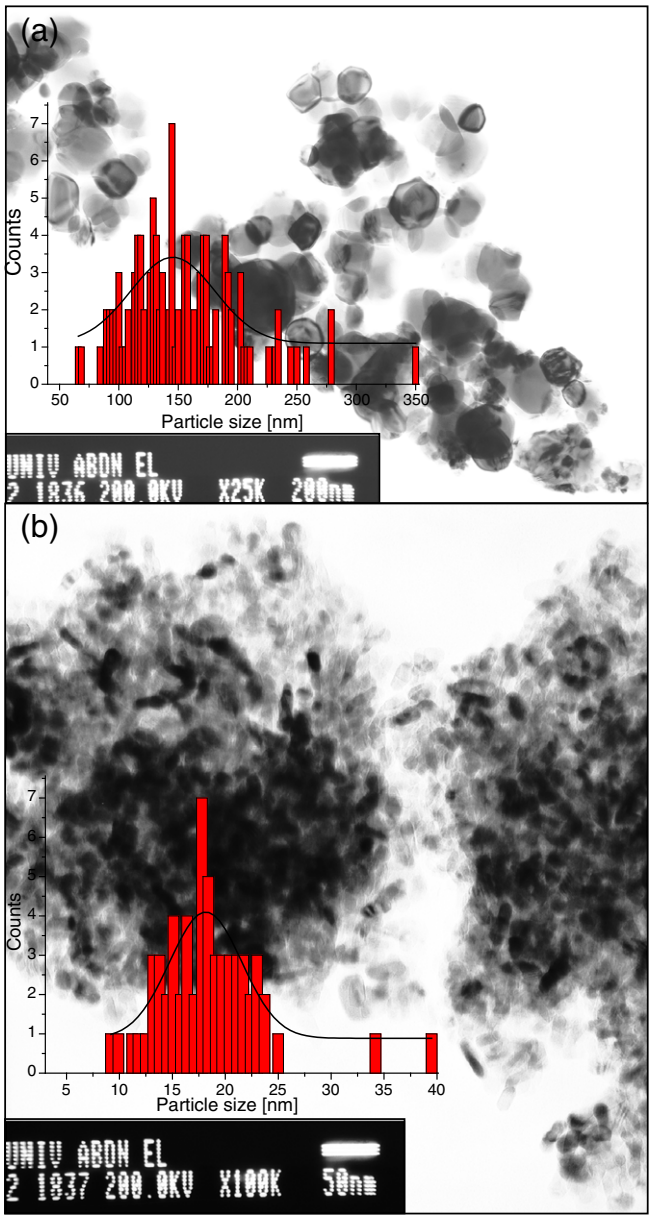

Fig. 8. T.E.M. micrographs and particle size distribution of: (a) m-TiO_2, and (b) n-TiO_2.

not depend on electron–hole recombination (Figs. 1 and 2) and ii) the activity loss due to electron–hole recombination is always in favour of n-TiO_2 since uniquely depends on primary particle size (crystallites size), a possible explanation could be that once introduced in cement the actual surface area *available* for RhB adsorption is *not* the BET specific surface area measured on the two powders and m-TiO_2 could offer a higher surface for RhB adsorption than n-TiO_2. Precise evaluations of such available surface areas are extremely difficult to achieve; nevertheless speculations can be done observing the dispersion of the two titania samples in cement using SEM-EDS (see section *TiO_2 dispersion in hardened cement: a particle agglomeration model*).

3.3. Depollution: NOx oxidation

Fig. 13 shows the nitric oxide, NO, nitrogen dioxide, NO_2 and total nitrogen oxides, $NOx = NO + NO_2$, concentration profiles obtained during the NOx oxidation test at three different flow rates and under illumination. In each graph trends obtained with photocatalytic cement mortars (either with m-TiO_2 or n-TiO_2) are compared to trends exhibited by TiO_2-free white cement mortars. The flat character of profiles where TiO_2 is not present indicates very low impact on NO and NO_2 oxidation by the cement environment itself and/or eventual not catalysed photooxidation. Trends also suggest that the lower the flow rate (i.e. the higher the average gas transit time) the lower the NO and NO_2 final concentrations (at 90 min) hence the higher the conversions.

This is more evident in Fig. 14 (a) where the total NOx conversions at 90 min are plotted versus the gas flow rate. The decrease of the conversion with the increase of the flow rate indicates that 90 min of reaction time are not enough to reach the *actual* steady state (conversion constant at different flow rates). The comparison between photocatalytic activities of mortars containing either m-TiO_2 or n-TiO_2 suggests that n-TiO_2 generally performs better than m-

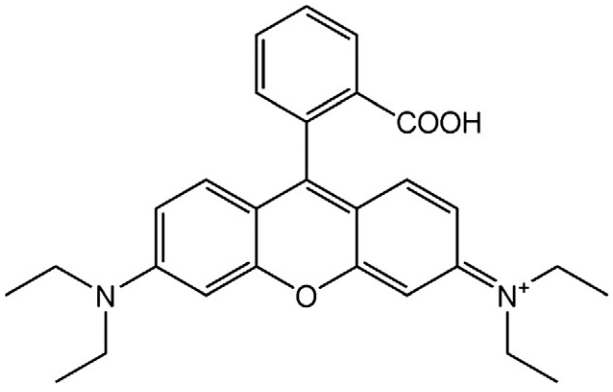

Fig. 9. Rhodamine B structure.

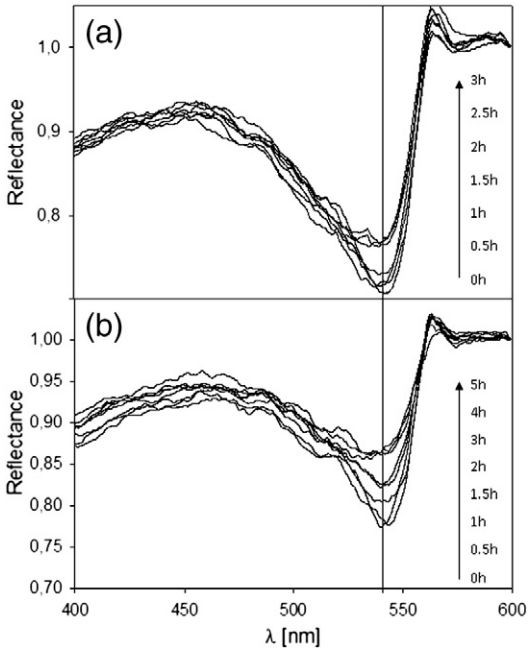

Fig. 10. Diffuse reflectance spectra at various illumination time for white cement pastes without photocatalyst: (a) RhB deposition and conditioning under daylight, and (b) RhB deposition and conditioning in darkness.

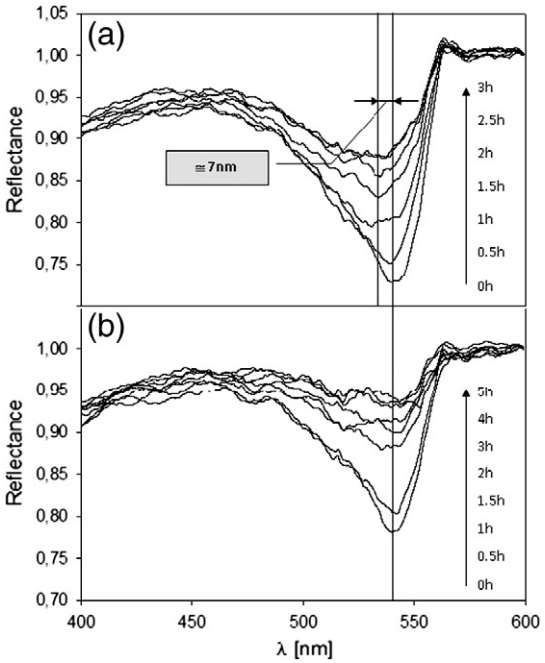

Fig. 12. Diffuse reflectance spectra at various illumination time for white cement pastes containing n-TiO_2: (a) RhB deposition and conditioning under daylight, and (b) RhB deposition and conditioning in darkness.

TiO_2. This reflects the values calculated for the photonic efficiencies (Fig. 14 (b)), being 0.10% for n-TiO_2 and 0.08% for m-TiO_2. The calculated photonic efficiencies seem to be in the same range as the ones reported by Kalousek et al. [47] on very similar systems. In this case (NOx oxidation), results are in agreement with what expected on the basis of the different BET specific surface areas of the two TiO_2 powders, which however failed to explain the higher activity towards RhB degradation exhibited by samples containing m-TiO_2.

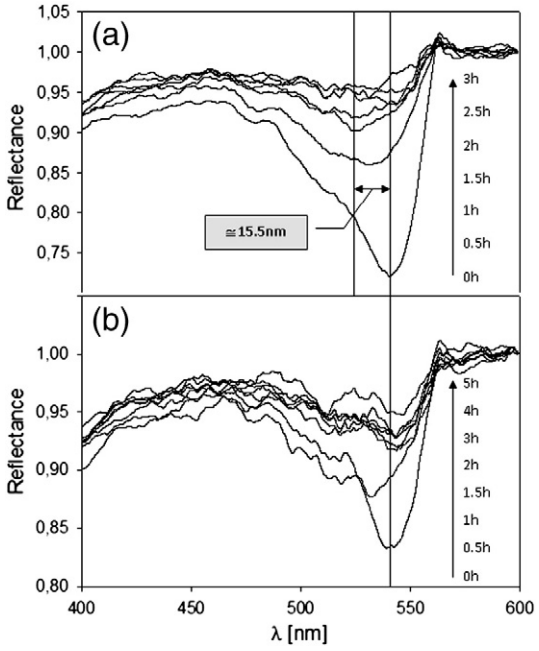

Fig. 11. Diffuse reflectance spectra at various illumination time for white cement pastes containing m-TiO_2: (a) RhB deposition and conditioning under daylight, and (b) RhB deposition and conditioning in darkness.

The analysis of the concentration profiles (Fig. 13) seems to indicate a very peculiar behaviour for the photocatalytic oxidation of NOx when TiO_2 is supported on cementitious materials (very high pH systems). The photocatalytic oxidation of NO on powder TiO_2 or TiO_2 supported on not high pH materials (e.g.: glass slides or beads, textile tiles, metal meshes, fabrics, etc.) is a complex series of chemical equilibria [28,35,48,49]. Adsorbed H_2O and O_2 react with light generated valence band positive holes and conductance band electrons on the surface of TiO_2 to form adsorbed hydroxyl radicals, HO , [28,35,48,49]. These radicals directly react with NO and, passing through nitrous acid, HONO, and nitrogen dioxide, NO_2, as intermediates, they convert NO into nitric acid, HNO_3, [28,35,48,49]. Since the reaction pathway occurs with a fast initial reactive photoadsorption ($NO \rightarrow HONO \rightarrow NO_2$) [48], the NO_2 concentration initially increases reaching a maximum and then decreases approaching a constant value (series of reaction kinetics). A very similar mechanism was supposed to be true for the case of cementitious materials containing TiO_2 where the very high pH would allow the formation of NO_2^- and NO_3^- rather than free HONO and HNO_3. However our experimental findings evidenced no presence of NO_2 initial concentration maxima. Although more experimental work needs to be done to fully understand this feature, some observations can be made considering the change of redox potentials of the nitrogen oxidation states in relation to change in pH. Fig. 15 shows the Frost diagram for the nitrogen oxidation states in acid and basic environments (courtesy of Rieger, Philip H., Electrochemistry, 2nd edition [50]). In the Frost diagram species corresponding to minima are expected to be thermodynamically stable since redox events from immediate nearby species are energetically downhill [50]. In acidic conditions the series $NO \rightarrow HONO \rightarrow N_2O_4$ ($\leftrightarrow 2NO_2$) $\rightarrow HNO_3$ do not show any increased stability states. All the species are highly reactive and the very high ΔG° for HNO_3 accounts for its high oxidative power. In alkaline conditions however both NO_2^- and NO_3^- are positioned in two minima with very similar ΔG°. This could imply that NO is mainly converted to NO_2^- and NO_2 to NO_3^- where the series of reaction above no longer occurs since NO_2^- shows a much higher redox stability. It is also interesting observing the feature of Eh versus pH

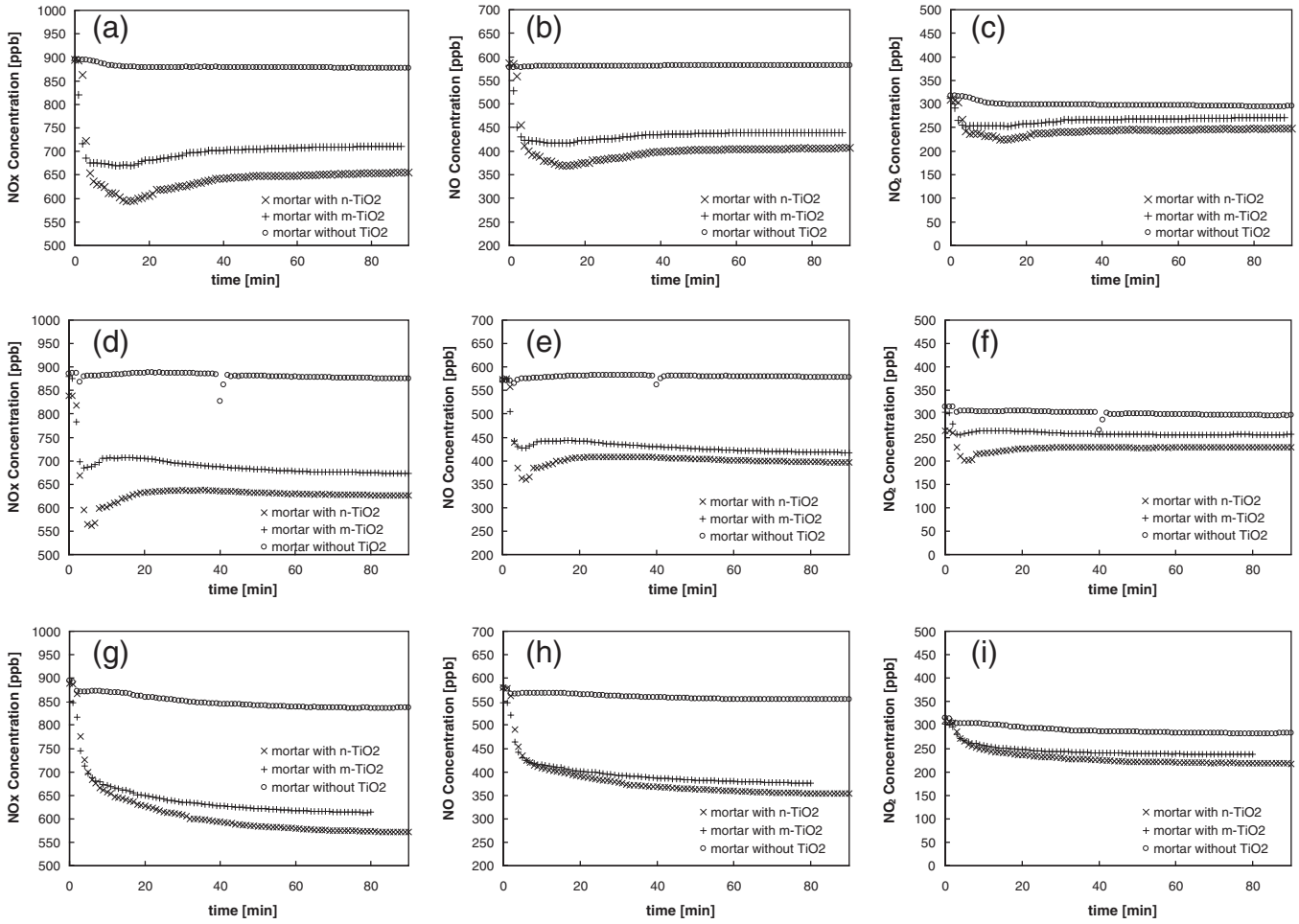

Fig. 13. NOx, NO and NO_2 concentration profiles at: (a), (b), (c) 3 l min^{-1}, (d), (e), (f) 2 l min^{-1}, (g), (h), and (i) 1.5 l min^{-1}.

diagram (Fig. 16, constructed using the Nernst equation) for N species when compared to the couple $OH^-/^{\bullet}OH$ (assuming $^{\bullet}OH$ as the main oxidant). Fig. 16 clearly shows that ΔEh between the couples $OH^-/^{\bullet}OH$ and N(II)/N(III), $OH^-/^{\bullet}OH$ and N(IV)/N(V) and $OH^-/^{\bullet}OH$ and N(III)/N(V) remain quite constant all over the pH domain, however, the ΔEh between the couples $OH^-/^{\bullet}OH$ and N(III)/N(IV) significantly reduces in highly alkaline environments, making this oxidation step (NO_2^- to NO_2) not as favourable as the others. The effect of the high pH could therefore be the potential switch off or inhibition of the step from N(III) to N(IV) in the overall oxidation mechanism (Fig. 17), hence accounting for the absence of initial maxima in NO_2 concentration profiles.

3.4. TiO_2 dispersion in hardened cement: a particle agglomeration model

In the attempt to understand the different activities exhibited by m- and n-TiO_2 towards RhB and NOx, a surface chemistry approach has been adopted. In a recent paper of the same authors [51] surface chemistry and electrokinetic properties of the two titania samples have been investigated. Coupling surface chemical analyses, ζ-potentials and surface charge densities profiles with sedimentation experiments in simulated cement pore solutions, have shown that in conditions of high pH and in the presence of non-indifferent electrolytes (e.g. Ca^{2+}) at high ionic activities (a typical cement environment), both m- and n-TiO_2 particles show tendency to surface overcharging and agglomeration due to ion-ion correlation phenomena [51–54]; similarly to C–S–H (calcium silica hydrates) particles in cement [55,56]. The structure of particle clusters due to enhanced agglomeration in cementitious environment is however very different if comparing m-TiO_2 with n-TiO_2 [51]. m-TiO_2 agglomerates are smaller, with bigger pores and better dispersed than n-TiO_2 ones. A surface chemical modification (with phosphorous and potassium applied during manufacturing to enhance and control crystal growth as well as to improve dispersability in water systems [51]) together with the larger particle size exhibited by m-TiO_2 are responsible for the small, deflocculated and highly dispersed agglomerates observed relative to that for the smaller n-TiO_2 [51] which shows larger, flocculated and not well dispersed agglomerates [51]. The model in Fig. 18 and the SEM micrographs in Figs. 19 and 20 related to cement specimens containing TiO_2 show the agglomeration/dispersion features described above. On the basis of such experimental evidence, photocatalytic activities can be interpreted in terms of *available surface area* in the hardened structure rather than B.E.T. specific surface area of titania in powder form. Large molecules like RhB, with an average molecular diameter of about 1.6 nm [57], can penetrate only with difficulty the interior of a n-TiO_2 cluster (pore size around 8 nm), but readily can access m-TiO_2 clusters (see Table 1). Moreover, RhB does not penetrate inside the cement pore structure. The smaller and better dispersed m-TiO_2 clusters on the surface of the specimens (Figs. 19(a) and 20(a)) together with their macropores (Table 1), may offer a higher *available* surface area for adsorption and consequent reaction of big molecules like Rhodamine B than the bigger and poorly dispersed n-TiO_2 clusters. Conversely, gaseous NOx has much smaller dimensions, 100 pm–200 pm [58], and can easily penetrate both

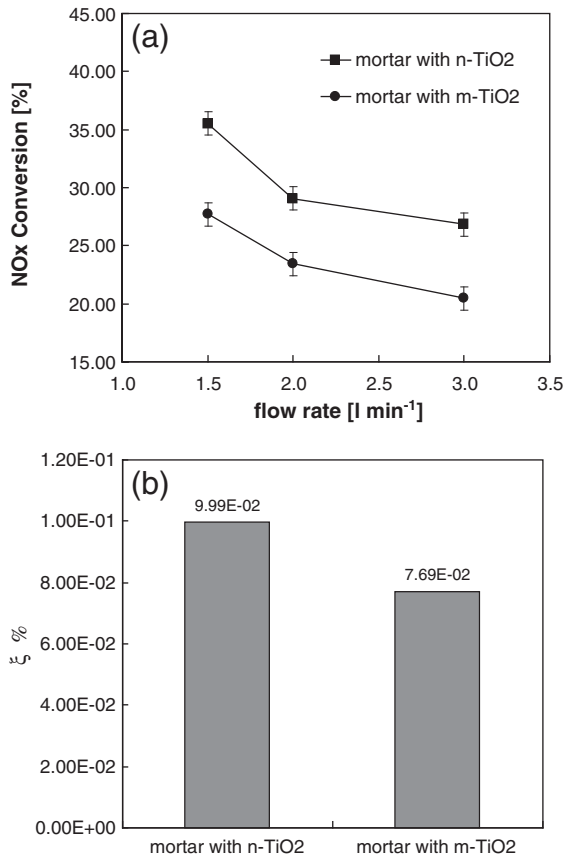

Fig. 14. NOx overall conversion versus flow rate for n-TiO_2 and m-TiO_2 (a). Photonic efficiency for n-TiO_2 and m-TiO_2 (b).

m-TiO_2 and n-TiO_2 clusters, accessing a higher surface area in both catalyst types; the higher specific surface of n-TiO_2 corresponds to the higher NOx degradation on this catalyst.

4. Conclusions

Application of TiO_2 photocatalysis to cement and concrete provides an efficient strategy to simultaneously obtain: self-cleaning effect of building facades, retardation of natural surface ageing as well as depollution of air, simply with the support of sunlight, atmospheric

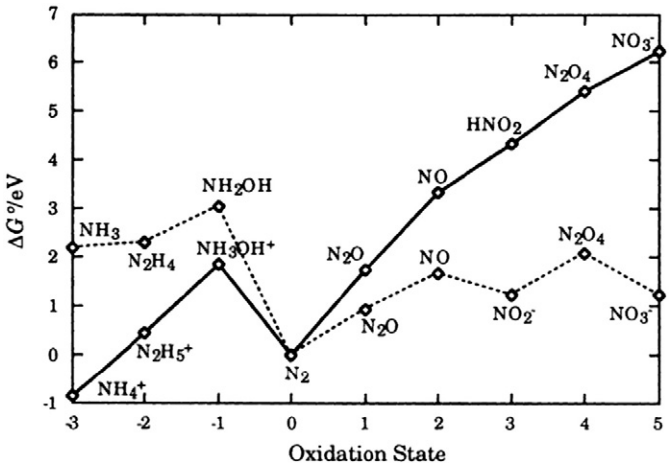

Fig. 15. Free energy-oxidation states diagram for the nitrogen oxidation states in acid (solid line) and basic (dashed line) solutions.

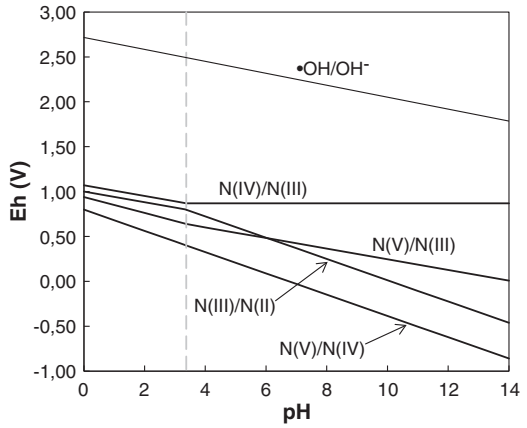

Fig. 16. Potential versus pH diagram showing the variation in half-cell potential with pH for the N(V)/N(IV), N(V)/N(III), N(IV)/N(III), N(III)/N(II) redox couples in comparison with the $^{\bullet}OH/OH^{-}$ redox couple. The vertical dashed line corresponds to the pKa of HONO.

oxygen and water present as humidity and/or rain water. In this paper, performances in degrading rhodamine B, RhB, (a common industrial test to evaluate self-cleaning activities) and performances in oxidising nitrogen oxide gaseous pollutants, NOx, are presented for two different TiO_2 samples (Table 1) tested in cement and mortars, together with an insight into the fundamental chemistry about TiO_2 photosensitised reactions responsible for the degradation processes involved.

Discolouration of RhB on TiO_2 in cement involves not only a proper photocatalytic mechanism (TiO_2-sensitised photoreaction) but also a dye-sensitised pathway. In the first mechanism light

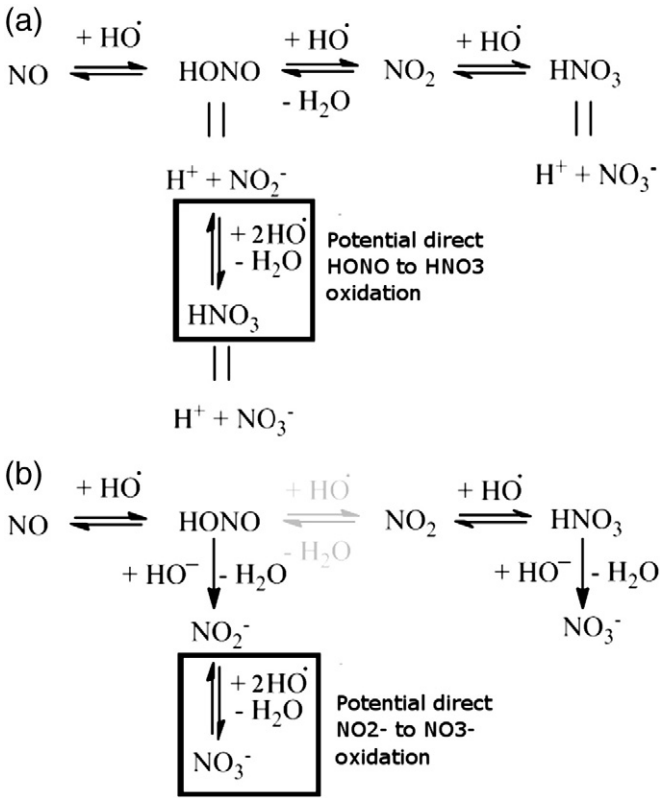

Fig. 17. Proposed mechanism of NOx oxidation on pure TiO_2 (a) [48] and on TiO_2 in mortar specimens (b). The equilibrium in grey indicates inhibition of the oxidative step.

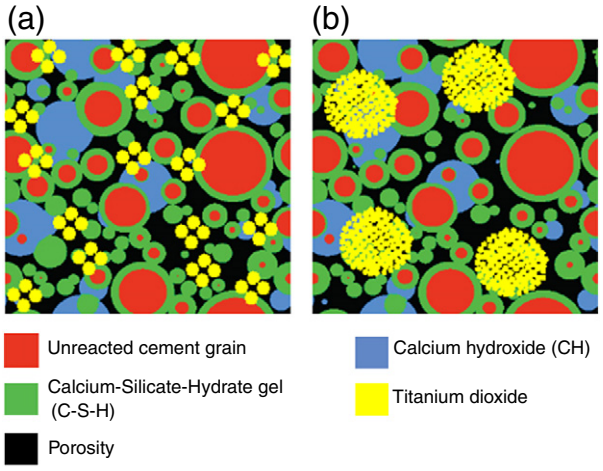

Fig. 18. Hardened cement structures with: (a) m-TiO_2 and (b) n-TiO_2.

activates TiO_2 through promotion of electrons from the valence band to the conductance band. Adsorbed water and oxygen react with valence band positive holes (left after promotion) and conductance band electrons respectively to generate hydroxyl radicals, HO, which ultimately degrade the adsorbed dye. In the second mechanisms, electrons in the HOMO level of the dye undergo transitions to the LUMO level and are subsequently injected into the conductance band of TiO_2. These electrons are therefore used by oxygen to generate oxidative species which degrade the already partially reacted dye.

The oxidation of NOx on the other hand uniquely follows a photocatalytic pathway, where nitric oxide, NO, and nitrogen dioxide, NO_2, are oxidised to nitrites, NO_2^-, and nitrates, NO_3^-. The very high pH typical of the cement environment seems to drive a different mechanism than the one occurring using powder TiO_2. The absence of initial maxima in the NO_2 concentration profiles would suggest that the step NO_2^- to NO_2, in the series of reactions typical of the case with powder TiO_2, might be inhibited.

In all these processes water and oxygen play a fundamental role since they are the precursors for the hydroxyl radicals, HO, and other oxygen-based species (e.g. peroxides, superoxides) responsible for mineralisation and oxidation of organics and inorganics.

The study has also linked photocatalytic performances to TiO_2 surface/colloidal chemistry and structure of TiO_2 clusters in cement. TiO_2 primary and secondary particle size, dispersion and agglomerate porosity in cement define accessible surface area. Big particle agglomerate pores, small and highly dispersed agglomerates of m-TiO_2 offer a higher *available* surface area for adsorption and reaction of big molecules like RhB which hardly penetrate n-TiO_2 particle

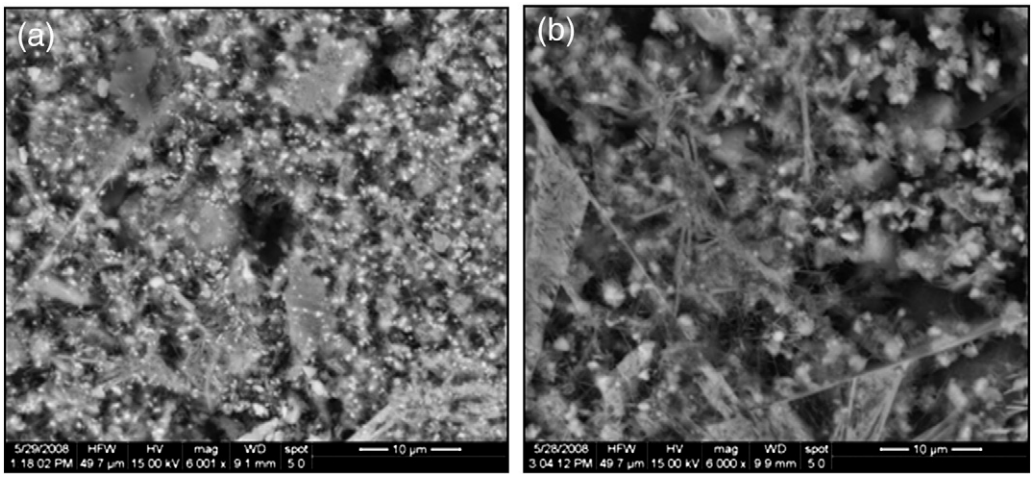

Fig. 19. SEM surface micrographs for cement specimens (1 day cured) prepared with: (a) m-TiO_2, and (b) n-TiO_2. SEM conditions adopted: no impregnation, no coating, low vacuum mode. The white spots in the micrographs indicate TiO_2 particle clusters. In the case of specimens prepared with m-TiO_2, clusters are smaller and better dispersed.

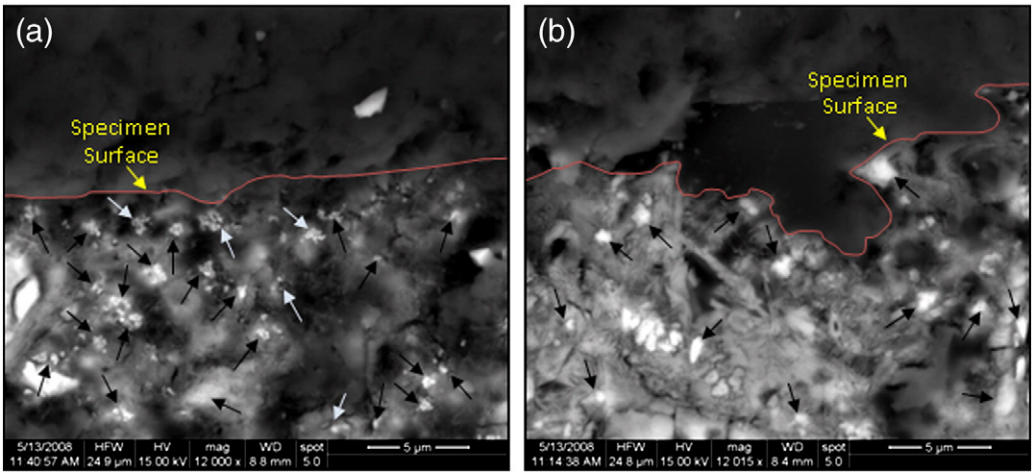

Fig. 20. SEM polished cross section micrographs for cement specimens (1 day cured) prepared with: (a) m-TiO_2, and (b) n-TiO_2. SEM conditions adopted: impregnation, no coating, low vacuum mode. The arrows in the micrographs indicate TiO_2 particle clusters.

agglomerate pores. On the other hand, very small molecules like nitrogen oxides which can easily penetrate into n-TiO_2 agglomerate pores too, are better degraded by n-TiO_2. Indeed in this case, dispersion and agglomerates porosity are not crucial; the available surface area is most likely to be due to the specific surface area determined by primary particle size.

Acknowledgment

The authors are grateful to the European Community under the Marie Curie Research Training Network MRTN-CT-2005-019283 "Fundamental understanding of cementitious materials for improved chemical physical and aesthetic performance" (http://www.nanocem.org/MC-RTN/) for the full support of Andrea Folli.

Appendix A. Supplementary data

Supplementary data to this article can be found online at doi:10.1016/j.cemconres.2011.12.001.

References

[1] A. Fujishima, K. Honda, Nature 238 (1972) 37–38.
[2] M.S. Wrighton, A.B. Ellis, P.T. Wolczanski, D.L. Morse, H.B. Abrahamson, D.S. Ginley, J. Am. Chem. Soc. 98 (1976) 2774.
[3] A. Fujishima, K. Hashimoto, T. Watanabe, TiO_2 Photocatalysis: Fundamentals and Application, 1 ed. BKC, Tokyo, 1999.
[4] H. Irie, S.P. Tee, T. Shibata, K. Hashimoto, Photo-induced Wettability Control on TiO2 Surface, Electrochem. Solid-State Lett. 8 (2005) 23–25.
[5] R. Wang, K. Hashimoto, A. Fujishima, M. Chikuni, E. Kojima, K. Kitamura, M. Shimohigoshi, T. Watanabe, Light-induced amphiphilic surfaces, Nature 338 (1997) 431–432.
[6] D. Rimmer, K.D. Sanderson, T. Paul, Coated glass, WO/2004/108619, , 2010.
[7] R. Cucitore, S. Cangiano, L. Cassar, High durability photocatalytic paving for reducing urban polluting agent, WO/2006/000565, , 2006.
[8] Y. Murata, H. Tawara, H. Obata, K. Murata, NOX-cleaning paving block, EP0786283, 2003.
[9] L. Cassar, A. Beeldens, N. Pimpinelli, G.L. Guerrini, Photocatalysis of cementitious materials, in: L. Cassar, P. Baglioni (Eds.), International RILEM Symposium on Photocatalysis, Environment and Construction Materials, RILEM, Florence, 2007, pp. 131–145.
[10] G.L. Guerrini, A. Plassais, C. Pepe, L. Cassar, Use of photocatalytic cementitious materials for self-cleaning applications, in: L. Cassar, P. Baglioni (Eds.), International RILEM Symposium on Photocatalysis, Environment and Construction Materials, RILEM, Florence, 2007, pp. 219–226.
[11] Determinazione dell'attività fotocatalitica di leganti idraulici - Metodo della Rodammina B., UNI, 11259, 2008, pp. 1–6.
[12] T. Wu, G. Liu, J. Zhao, H. Hidaka, N. Serpone, Photoassisted Degradation of Dye Pollutants. V. Self-Photosensitized Oxidative Transformation of *Rhodamine B* under Visible Light Irradiation in Aqueous TiO_2 Dispersions. J. Phys. Chem. B 102 (1998) 5845–5851.
[13] F. Chen, J. Zhao, H. Hidaka, Highly selective deethylation of rhodamine B: Adsorption and photooxidation pathways of the dye on the TiO_2/SiO_2 composite photocatalyst, Int. J. Photoenergy 5 (2003) 209–217.
[14] J. Li, L. Li, L. Zheng, Y. Xian, L. Jin, Photoelectrocatalytic degradation of rhodamine B using Ti/TiO_2 electrode prepared by laser calcination method, Electrochim. Acta 51 (2006) 4942–4949.
[15] J. Li, W. Ma, P. Lei, J. Zhao, Detection of intermediates in the TiO_2-assisted photodegradation of Rhodamine B under visible light irradiation, J. Environ. Sci. 19 (2007) 892–896.
[16] E.T. Soares, M.A. Lausarin, C.C. Moro, A study of process variables for the photocatalytic degradation of Rhodamine B, Braz. J. Chem. Eng. 24 (2007) 29–36.
[17] A. Mills, S. Le Hunte, An overview of semiconductor photocatalysis, J. Photochem. Photobiol., A 108 (1997) 1–35.
[18] R.M. Harrison, Pollution: causes, effects and control, 2 ed. The Royal Society of Chemistry, Cambridge, 1992.
[19] D. Elsom, Atmospheric Pollution, 1 ed. Basil Blackwell, New York, 1987.
[20] J.H. Seinfeld, Atmospheric chemistry and physics: from air pollution to climate change, 1 ed. Wiley, New York, 1998.
[21] F.A. Cotton, G. Wilkinson, Advanced Inorganic Chemistry, 5 ed. Wiley-Interscience, USA, 1988.
[22] C.A. Latta, Plant Eng. 52 (1998) 105–112.
[23] S.K. Gangwal, G.B. Howe, J.J. Spivey, P.L. Silveston, R.R. Hudgins, J.G. Metzinger, Environ. Prog. 12 (1993) 128.
[24] A. Beeldens, Air purification by road materials: results of the test project in Antwerp, in: L. Cassar, P. Baglioni (Eds.), International RILEM Symposium on Photocatalysis, Environment and Construction Materials, RILEM, Florence, 2007, pp. 187–194.
[25] D.H. Chen, K. Li, Photocatalytic Coating on Road Pavements/Structures for NOx Abatement, Lamar University Report, 2007, pp. 1–17.
[26] S. Chen, G. Cao, Study on the photocatalytic oxidation of NO_2^- ions using TiO_2 beads as a photocatalyst, Desalination 194 (2006) 127–134.
[27] J.S. Dalton, P.A. Janes, N.G. Jones, J.A. Nicholson, K.R. Hallam, G.C. Allen, Photocatalytic oxidation of NOx gases using TiO_2: a surface spectroscopic approach, Environ. Pollut. 120 (2002) 415–422.
[28] S. Devahasdin, C.J. Fan, K. Li, D.H. Chen, TiO2 photocatalytic oxidation of nitric oxide: transient behavior and reaction kinetics, J. Photochem. Photobiol., A 156 (2003) 161–170.
[29] G.L. Guerrini, E. Peccati, Photocatalytic cementitious roads for depollution, in: L. Cassar, P. Baglioni (Eds.), International RILEM Symposium on Photocatalysis, Environment and Construction Materials, RILEM, Florence, 2007, pp. 179–186.
[30] H. Ichiura, T. Kitaoka, H. Tanaka, Photocatalytic oxidation of NOx using composite sheets containing TiO_2 and a metal compound, Chemosphere 51 (2003) 855–860.
[31] M. Kawakami, T. Furumura, H. Tokushige, NOx removal effects and physical properties of cement mortar incorporating titanium dioxide powder, in: L. Cassar, P. Baglioni (Eds.), International RILEM Symposium on Photocatalysis, Environment and Construction Materials, RILEM, Florence, 2007, pp. 163–170.
[32] D. Ollis, H. Al-Ekabi, Photocatalytic purification and treatment of water and air, Elsevier, New York, 1993.
[33] C.S. Poon, E. Cheung, NO removal efficiency of photocatalytic paving blocks prepared with recycled materials, Constr. Build. Mater. 21 (2006) 1746–1753.
[34] Determination of the degradation of nitrogen oxides in the air by inorganic photocatalytic materials: continuous flow test method, UNI, 11247, 2009, pp. 1–11.
[35] H. Wang, Z. Wu, W. Zhao, B. Guan, Photocatalytic oxidation of nitrogen oxides using TiO2 loading on woven glass fabric, Chemosphere 66 (2007) 185–190.
[36] J. Zhao, X. Yang, Photocatalytic oxidation for indoor air purification: a literature review, Build. Environ. 38 (2003) 645–654.
[37] TX Actice Applications - pavements (Italcementi Group), http://www.italcementi.it/ITA/Prodotti+servizi+e+qualita/Prodotti+Fotocatalitici/Realizzazioni/Gallerie_Realizzazioni/Pavimentazioni.htm.
[38] Highland Park, Illinois (Essroc, Italcementi Group), http://txactive.us/images/ESSROC_Press_Release_Hyacinth.pdf.
[39] G. Hüsken, M. Hunger, H.J.H. Brouwers, Comparative study on cementitious products containing titanium dioxide as photo-catalyst, in: L. Cassar, P. Baglioni (Eds.), International RILEM Symposium on Photocatalysis, Environment and Construction Materials, RILEM, Florence, 2007, pp. 147–154.
[40] H. Lin, C.P. Huang, W. Li, C. Ni, S. Ismatshah, Y. Tseng, Size dependency of nanocrystalline TiO_2 on its optical property and photocatalytic reactivity exemplified by 2-chlorophenol, Appl. Catal., B 68 (2006) 1–11.
[41] S. Brunauer, P.H. Emmett, E. Teller, J. Am. Chem. Soc. 60 (1938) 309–319.
[42] E.P. Barrett, L.G. Joyner, P.P. Halenda, J. Am. Chem. Soc. 73 (1951) 373–380.
[43] Cement - Test methods - Determination of strength, ISO, 679, 2009, pp. 1–30.
[44] Bruker AXS Inc., DIFFRACplus EVA - Bruker X-ray diffraction pattern database software, Madison, WI; Version 7, 2002.
[45] E. Dowty, ATOMS_Software. First publication 1989. Version 6.4, 2011.
[46] A. Folli, U.H. Jakobsen, G.L. Guerrini, D.E. Macphee, Rhodamine B Discolouration on TiO2 in the Cement Environment: A Look at Fundamental Aspects of the Self-cleaning Effect in Concretes, J. Adv. Oxid. Technol. 12 (2009) 126–133.
[47] V. Kalousek, J. Tschirch, D. Bahnemann, J. Rathouský, Mesoporous layers of TiO2 as highly efficient photocatalysts for the purification of air, Superlattices Microstruct. 44 (2008) 506–513.
[48] A. Folli, S.B. Campbell, J.A. Anderson, D.E. Macphee, Role of TiO2 surface hydration on NO oxidation photo-activity, J. Photochem. Photobiol., A 220 (2011) 85–93.
[49] K. Hashimoto, K. Wasada, N. Toukai, H. Kominami, Y. Kera, Photocatalytic oxidation of nitrogen monoxide over titanium(IV) oxide nanocrystals large size areas, J. Photochem. Photobiol., A 136 (2000) 103–109.
[50] P.H. Rieger, Electrochemistry, 2nd ed. Chapman and Hall, New York, 1994.
[51] A. Folli, I. Pochard, A. Nonat, U.H. Jakobsen, A.M. Shepherd, D.E. Macphee, Engineering photocatalytic cements: understanding TiO2 surface chemistry to control and modulate photocatalytic performances, J. Am. Ceram. Soc. 93 (2010) 3360–3369.
[52] C. Labbez, B. Jönsson, M. Skarba, M. Borkovec, Ion-ion correlation and charge reversal at titrating solid interfaces, Langmuir 25 (2009) 7209–7213.
[53] B. Jönsson, H. Wennerström, Ion-ion correlations in liquid dispersions, J. Adhes. 80 (2004) 339–364.
[54] F. Mange, P. Couchot, A. Foissy, A. Pierre, J. Colloid Interface Sci. 159 (1993) 58–67.
[55] B. Jönsson, A. Nonat, C. Labbez, B. Cabane, H. Wennerström, Controlling the cohesion of cement paste, Langmuir 21 (2005) 9211–9221.
[56] C. Labbez, A. Nonat, I. Pochard, B. Jönsson, Experimental and theoretical evidence of overcharging of calcium silicate hydrate, J. Colloid Interface Sci. 309 (2007) 303–307.
[57] C.H. Hou, X. Wang, C. Liang, S. Yiacoumi, C. Tsouris, S. Dai, Molecular-Sieving Capabilities of Mesoporous Carbon Membranes, J. Phys. Chem. B 112 (2008) 8563–8570.
[58] A.F. Wells, Structural Inorganic Chemistry, 5th ed. Oxford University Press, Oxford, UK, 1984.